Locally adaptive temperature response of vegetative growth in *Arabidopsis thaliana*

Pieter Clauw[1,✉], Envel Kerdaffrec[2], Joanna Gunis[1], Ilka Reichardt[3], Viktoria Nizhynska[1], Stefanie Koemeda[4], Jakub Jez[4], and Magnus Nordborg[1,✉]

[1]Gregor Mendel Institute of Molecular Plant Biology, Austrian Academy of Sciences, Vienna BioCenter (VBC), 1030 Vienna, Austria
[2]Department of Biology, University of Fribourg, CH-1700 Fribourg, Switzerland
[3]Max Planck Institute of Molecular Cell Biology and Genetics, Dresden, 01307 Dresden, Germany
[4]4 Plant Sciences Facility, Vienna BioCenter Core Facilities GmbH (VBCF), 1030 Vienna, Austria

We investigated early vegetative growth of natural *Arabidopsis thaliana* accessions in cold, non-freezing temperatures, similar to temperatures these plants naturally encounter in fall at northern latitudes. We found that accessions from northern latitudes produced larger seedlings than accessions from southern latitudes, partly as a result of larger seed size. However, their subsequent vegetative growth when exposed to colder temperatures was slower. The difference was too large to be explained by random population differentiation, and is thus suggestive of local adaptation, a notion that is further supported by substantial transcriptome and metabolome changes in northern accessions. We hypothesize that the reduced growth of northern accessions is an adaptive response, and a consequence of reallocating resources towards cold acclimation and winter survival.

Correspondence:
pieter.clauw@gmi.oeaw.ac.at
magnus.nordborg@gmi.oeaw.ac.at

Introduction

Plants use a wide variety of life-history strategies in adaptation to their local environment. These strategies have evolved to maximize fitness, but are constrained by trade-offs between components such as growth, survival and reproduction (1, 2). While most life-history studies investigate differences between species, there is also variation found within species, including in *Arabidopsis thaliana*, where life-history variation has been linked to climate parameters (3–5). Less clear is how trade-offs are shaping this variation. In this paper we consider vegetative growth, a key component of life history, and use transcriptome and metabolome data to help explore potential trade-offs. We did this specifically in cold temperatures meant to simulate natural conditions in the northern regions of the species distribution.

Local adaptation studies in *A. thaliana* have found important roles for life-history traits such as seed dormancy and flowering time (6). Temperature is a major regulator of these traits and local populations are adapted to their local climate (7–9). Plant growth is also affected by temperature, and previous studies have detected genetic variation underlying growth-related traits (10, 11) as well as signals of polygenic adaptation (12). How vegetative growth is adapted to local temperatures remains unclear, however.

Growth can be seen as the end-sum of a vast number of physiological processes. All of these are genetically determined but can also be heavily influenced by environmental conditions. Growth is therefore not only genetically a complex trait but also enormously plastic. The most straightforward environmental effect is when conditions are so adverse that growth reaches a physiological limit, making it impossible for the plant to grow any further. This is called "passive plasticity" (13, 14). Yet, when survival is at stake, it may also be in the interest of the plant to actively inhibit growth upon deteriorating environmental conditions (15), called "active plasticity" (13, 14). Since vegetative growth ultimately determines photosynthetic surface and thus energy input that can be invested in the next generation, it is directly related to fitness, and is typically in trade-off with survival. Allocation of resources towards either growth or survival is thus an important balance to keep, and plants are expected to be adapted to constantly perceiving and responding to specific environmental changes as cues for looming adverse conditions.

Cold acclimation is a well-studied mechanism in plants, in which decreasing temperatures induce freezing tolerance in preparation for winter (16, 17). This temperature response is typically studied at 4ºC, but has been observed in temperatures up to 12ºC (18). The increased freezing tolerance is accomplished by changing membrane composition, producing cryoprotective polypeptides such as COR15A (19, 20) and accumulating compatible solutes with cryoprotective properties such as raffinose, sucrose and proline (21–23). Main regulators of cold acclimation are CBF1/DREB1b, CBF2/DREB1c and CBF3/DREB1a, three AP2/ERF transcription factors, for which allelic variation in CBF2 has been linked to natural variation in freezing tolerance (24–26). Nothing is known, however, about whether natural variation in freezing tolerance regulation also influences a trade-off with growth responses to cold temperatures.

Here we investigated the role of growth in adaptation to cold temperatures by comparing vegetative growth of 249 accessions (Figure 1) grown in daily maximum temperatures of 16ºC and 6ºC for a period of 3 weeks following seedling establishment (Figure S1). Rosette growth of each plant was measured twice a day during temperature treatments, using automated phenotyping. The experiment generated rosette growth estimates at a high temporal resolution in two ecologically realistic temperature conditions in a wide set of accessions, allowing us to look for patterns of local adaptation.

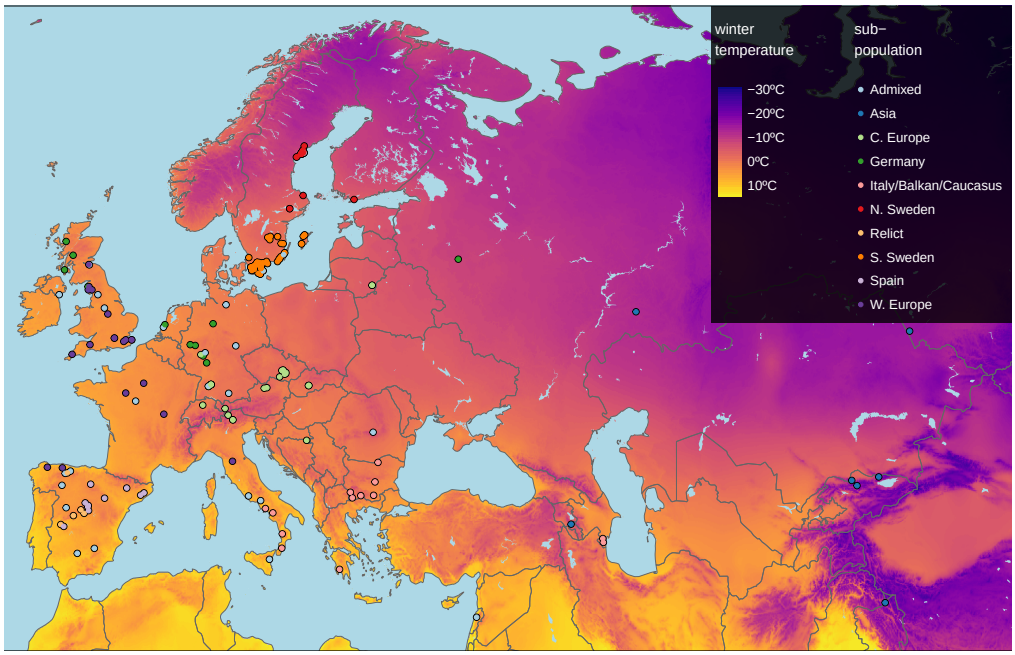

Fig. 1. Geographic origin of the 249 accessions. Map color shows winter temperature (mean temperature of coldest quarter). Accessions are colored according to subpopulation (27). Accessions from the warmest and coldest regions are from Greece and the Himalayas, respectively.

Results

Estimating plant growth parameters.

Our highly replicated experiment yielded dense (two measurements per day) time series growth data for over 7,000 individual plants (5 replicate plants X 249 accessions X 2 treatments X 3 replicate experiments). These data were used to model plant growth and estimate growth parameters for further analysis. Unlimited growth should be exponential, but plant growth is known to slow down with increasing size, and therefore a power-law function, $\frac{dM}{dt} = rM^{\beta}$, with $\beta < 1$ is typically a better fit than a pure exponential function (for which $\beta = 1$ — in the equation, M is the size, r is the growth rate, and β is a scaling factor that allows rate of size increase to change with size). Growth according to a power-law function typically describes early stages of plant growth especially well (28) and our rosette size measurements were no exception (see Materials and Methods). To calculate the rosette size from a power-law function at a given time point only three parameters are required: the initial size (M_0), growth rate (r), and β. Note that (M_0) is the rosette size at the start of the temperature treatment 14 days after stratification (Figure S1) and is thus not affected by the temperature treatment. We used a non-linear mixed model to obtain estimates for the initial size, growth rates and β. Accession was added as fixed effect for initial size and growth rate, temperature and accession X temperature interactions were added as fixed effects for growth rate only. β was considered to be constant over accessions and temperatures. The "temperature response" of the growth rate was calculated for each accession as the slope between the growth rate at 16ºC and 6ºC. As expected, all accessions grew faster when it was warmer. The observed phenotypic variation (Figure S2) is to a large extent explained by genetic variation; broad-sense heritabilities are 0.41 for initial size, and 0.57 and 0.32 for growth rate at 16ºC and 6ºC respectively.

Growth parameters correlate with the environment of origin.

If growth rates are locally adaptive, they may reflect the environment of origin of each accession. To investigate this, we correlated our estimated growth rates with climate data. The climate variables showing the strongest correlations with the different growth parameters were linked to winter temperatures (Figure S3), also when correlations were corrected for population structure (Figure S4). In particular, the mean temperature during the coldest quarter (henceforth referred to as "winter temperature") was most strongly correlated with our parameter estimates, and we focus on it in what follows.

Initial size.

Accessions from colder climates generally had higher initial rosette size (M_0), 2 weeks after germination, than accessions from warmer climates ($r = -0.39$; $p - value = 1.6e - 10$), but then grew more slowly during the temperature experiment — regardless of temperature regime (Figure 2; Figure S6). Because during the first two weeks the plants were growing at 21ºC, it is impossible to disentangle early growth from growth at a warmer temperature.

One reason for this pattern is likely to be differences in seed size between accessions. Using unpublished seed size measurements for a subset of 123 Swedish accessions from previous experiments, we found that seed size is positively correlated with initial size ($r = 0.28$; $p - value = 0.0014$; Figure S5A), and also with winter temperature ($r = -0.75$; $p - value = 2.2e - 16$; Figure S5), at least for the subset of 123 Swedish accessions. In a random effect model, winter temperature explained 32.7% of the variation in initial size,

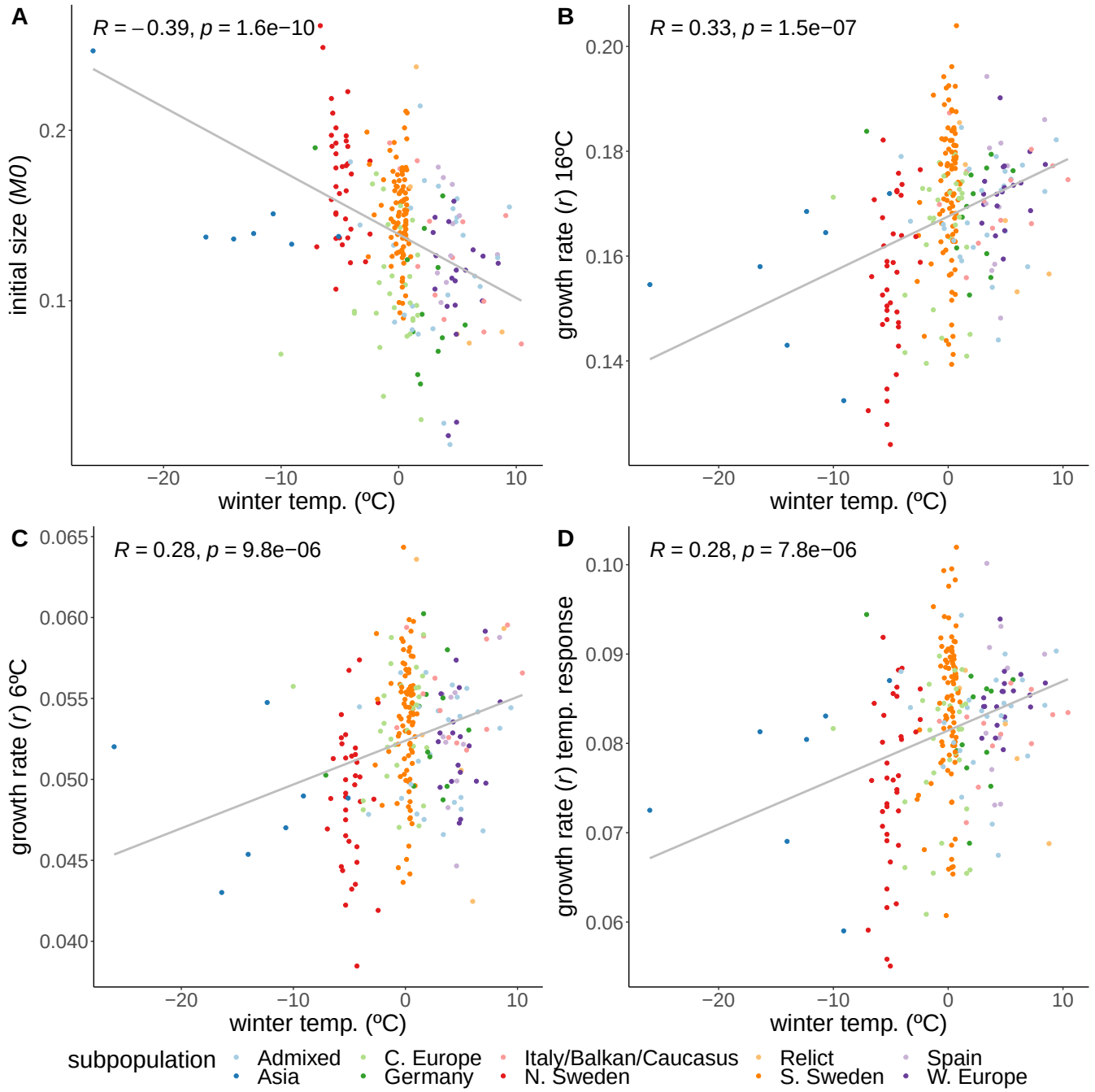

Fig. 2. Correlations of growth parameters with winter temperature. Colors indicate genetically defined subpopulations of the accessions (27).

whereas seed size explained 11.9%. Winter temperature is still significantly associated with initial size when seed size is taken into account ($p-value < 1e-04$). The precise role of seed size in initial growth is surely a topic that would benefit from further studies, but for the purpose of this study, it is clear that seed size alone cannot explain the geographic pattern we observe for M_0 and that there must be a role for variation in growth rate during the very initial phases of seedling growth.

Growth rates.

While the initial sizes correlate negatively with winter temperature, we observed the opposite relation for the growth rates. Despite being larger initially, accessions from colder climates grew more slowly during both the 16ºC ($r = 0.33$; $p-value = 1.5e-7$) and 6ºC ($r = 0.28$; $p-value = 9.8e-6$) treatments (Figure 2). The higher growth rates of accessions from warmer climates prove that resources are not limiting, suggesting that the northern lines are actively inhibiting their growth, and that growing slower may be beneficial in colder climates, perhaps in preparation for winter. Accessions from colder climates were also less sensitive to the temperature experiment in the sense that the temperature response of the growth rate increased with winter temperature of origin ($r = 0.28$; $p-value = 7.8e-6$; Figure 2). Even though accessions from the Asian and North-Swedish sub-

populations were more variable in their growth rate temperature response (Figure S7A), the correlations still hold when removing either Asian or northern and southern Swedish subpopulations (Figure S7B; Figure S6D), and when looking specifically within the northern and southern Swedish subpopulations (Figure S7C).

Cold acclimation response

Just like the observed geographic pattern of the growth rates, metabolite measurements taken at the final day of our experiment showed clear differences between accessions from cold and warm regions, and many of these differences involved metabolites with a known role in cold acclimation (29). Since the transcriptomic component of cold acclimation is well studied, we analyzed the expression profiles of 251 previously described cold acclimation genes (Supplemental Dataset 2) in 8 accessions that were representative in terms of their growth and metabolome profiles (Figure S8). The selected genes are described in the literature as being differentially expressed upon exposure to cold, and their expression is under control of at least one of the known transcription factors regulating cold acclimation: CBF1, CBF2, CBF3, HSFC1 (30) or ZAT12 (31). In our experiment, expression of these genes is likewise more affected by temperature than expected by chance (Figure 3; χ^2-test: $p-value < 0.001$), and separates the two accessions from the coldest region (northern Sweden) from the rest in the 16ºC treatment, and the three accessions from the warmest regions (Spain and Azerbaijan) from the rest in the 6ºC treatment. Expression of different subsets of the selected cold-acclimation genes show clear correlations with winter temperature of origin (Figure S9). In particular, the genes that were previously found to be up-regulated upon cold exposure showed higher expression in accessions from cold climates (Figure S11). Since the expression of these cold acclimation genes is linked to the strength of cold acclimation, these accessions likely differ in their ability to cope with freezing temperatures upon cold treatment.

Growth is polygenic and shows signs of local adaptation

We used genome-wide association to investigate the genetic architecture underlying variation for the different growth parameters. As expected, these traits appear to be highly polygenic, and there were no genome-wide significant associations (Figure S12). The strongest association was found for overall growth rate in 16ºC (Figure 4A). Inflated significance levels after correcting for population structure are consistent with what we would expect from a polygenic trait (Figure 4B) and were also observed for the other traits, except for growth rate in 6ºC (Figure S12). Plausible candidates within 10kb of the most significant SNP (chr5:23,334,281; $-log_10(p-value) = 6.85$; effect size $= -0.00913 \pm 0.00169$) include *CIPK21* and *MYB36*. *CIPK21* encodes a CBL-interacting protein kinase that is upregulated in cold conditions and is involved in the salt and osmotic stress response (32). MYB36

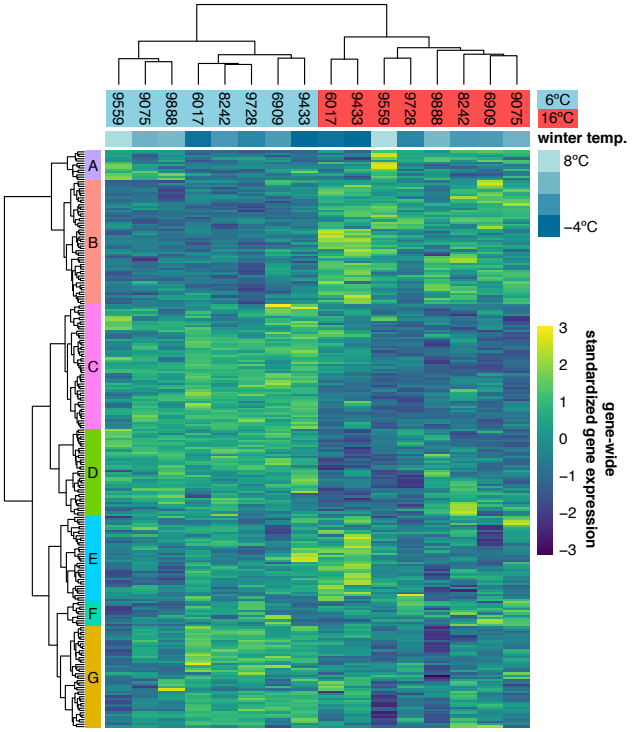

Fig. 3. Expression of 251 previously described cold acclimation genes. Expression is shown as the gene-wide z-scores of the normalized counts. The z-scores allow for grouping genes with a similar expression behavior over the different accessions in both temperatures. The top bar indicates winter temperature (ºC) for each accession's origin. Both dendrograms along y-axis and x-axis respectively show hierarchical clustering of genes, and of accessions in both temperatures.

is a key regulator of root endodermal differentiation (33). Slightly more distant, 22kb away, is $COL5$, encoding a transcription factor that is part of the gene network that is regulated by AN3, a regulator of cell proliferation in leaf growth (34).

To test for potential polygenic adaptation, we compared the phenotypic divergence to the expected neutral genome-wide genetic divergence. This can be done using an $Q_{ST} - F_{ST}$ test (35–37), however this test is not well suited for species with complex population structure, and so we used a variation that was designed to detect adaptive differentiation for traits measured in structured GWAS panels (38). Instead of looking at divergences between predefined populations, this method uses principal components (PCs) of the genetic relatedness matrix as axes of potential adaptive differentiation. Adaptive differentiation is then detected as a correlation between the focal phenotype and any of these relatedness PCs that is significantly different than expected under neutrality. Adaptive differentiation was detected for initial size and for growth rate in 16ºC and its temperature response. Both traits show adaptive differentiation along different genetic axes (Figure 5). Initial size shows significant adaptive differentiation along PC6 ($p-value < 0.05$), whereas growth rate in 16ºC and its temperature response showed significant adaptive differentiation along PC5 ($p-values < 0.05$). Adaptive differentiation was not significant along the other axes of genetic differentiation (PC1-4, PC7-10). The adaptive differentiation for initial size along PC6 seems to stem from higher

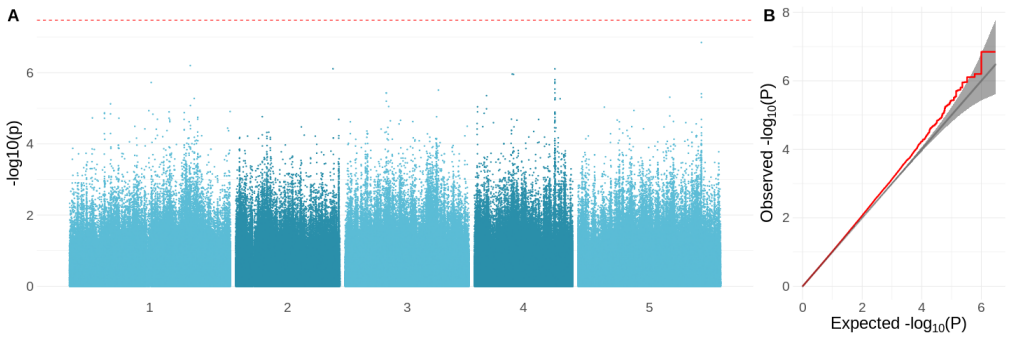

Fig. 4. GWAS results for the growth rate in 16ºC. A: Manhattan plot showing the significance of the association between the phenotype and each of the tested SNPs ($MAF > 10\%$). The Bonferroni-corrected threshold is shown with a dashed red line. B: QQ-plot showing the relation between observed and expected $-log10(p-value)$ distributions. Red line shows the observed relationship. The gray line and band show the expected relationship under the null hypothesis of no differentiation between both distributions.

initial sizes in Swedish accessions, compared to central European accessions. The adaptive differentiation along PC5 seems to be driven by the lower growth rate temperature responses in Asian and northern Swedish accessions in contrast to higher growth rates in a subset of southern Swedish accessions. The accessions in our set that come from northern Sweden and Asia hail from the coldest climates. Thus these results suggest adaptive differentiation driven by adaptation to cold winters. Given the seemingly strong influence from the Asian accessions we repeated the analysis without them. Also in this analysis we detected significant adaptive differentiation ($p-values < 0.05$) for initial size, growth rate in 16ºC and its temperature response (Figure S13).

Discussion

This study explores natural variation of rosette growth in non-freezing temperatures. We detect genetic variation for the different growth parameters, and environmental correlations that suggest local adaptation. GWAS analyses reveal, not surprisingly, a polygenic trait architecture. Indeed, across the genome we detect adaptive differentiation for certain growth parameters. We speculated that the slower growth measured in accessions from colder climates reflect relocation of resources from growth towards cold acclimation. Both metabolome and gene expression data are consistent with accessions from colder climates preparing for a harsh winter. In our temperature experiment, we see that the growth of northern lines is affected less than southern lines by switching from 16ºC to 6ºC.

Our conclusion that slower growth is likely adaptive in populations facing fiercer winters is in line with recent results of (12), who concluded that the reduced growth in Northern lines was adaptive and not a consequence of an accumulation of deleterious mutations at the species border. If slower growth were indeed a consequence of accumulated deleterious mutations we would expect to see slower growth also during the initial seedling establishment, which we measured here as the initial size. On the contrary, we saw a fast seedling establishment for accessions from colder regions. We speculate that the fast seedling establishment is a potential adaptation for short growth seasons, which often coincide with colder climates (high latitude or high altitude). This fast seedling establishment seems to be partly supported by larger seeds. These larger seeds may provide more nutrients to initiate faster seedling establishment, while this is of less importance in warmer climates with longer growth seasons. Further work is needed to disentangle initial growth from seed size effects and confirm that there is a causal relationship between seed size and fast seedling establishment, whether this is due to seed nutrient storage, and whether it is adaptive.

The adaptation of growth to local climates is likely to be influenced by a trade-off with cold acclimation. General growth-survival trade-offs have long been observed and are described in general ecological strategy schemes such as Grime's C-S-R triangle (39) and the leaf-height-seed scheme (40). Specific trade-offs between growth and cold/frost survival were observed for wheat (41, 42), alfalfa (43), *Dactylis glomerata* (44), and multiple tree species (45–48). Here we observed higher expression of genes involved in cold acclimation in accessions from colder regions. This is clearest in 6ºC, but is also happening in 16ºC, suggesting that activation of cold acclimation is stronger in accessions from cold climates and may be triggered more easily. Accessions from warm climates may instead activate cold acclimation as a stress response rather than as a preventive measure. Even though this is based on a limited set of 8 accessions, metabolome measurements in all 249 accessions lead to the same conclusion. Metabolites involved in cold acclimation such as raffinose, sucrose and proline were found in higher concentrations in accessions from colder climates (29). We believe that accessions from colder environments are relocating more energy and resources from growth towards preparations for upcoming freezing temperatures, which is a clear example of active plasticity (13, 14). This likely results in stronger cold acclimation and consequently increased freezing tolerance in the accessions from colder regions. Indeed, accessions originating from colder environments show increased freezing tolerance upon cold acclimation (49–52). This fits with observations of northern and colder regions favoring slower growing, more stress-tolerant plants (3, 4). Also biogeographic studies in *A. thaliana* found that winter temperatures are a major determinant of suitable habitats for this species (53–55). The high variability we observed in our data does, however, show that there is more at play than selec-

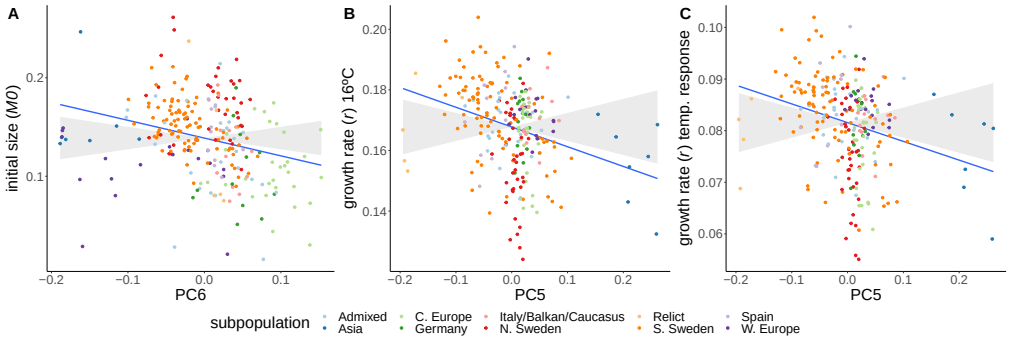

Fig. 5. Adaptive differentiation of initial size, growth rate at 16ºC, and the temperature response of growth rate along different axes of genetic differentiation. Accessions are coloured according to their respective admixture groups, as specified in (27). The gray ribbon represents the expected correlation between phenotype and axis of genetic differentiation under neutrality with a 90% confidence interval. The neutral expectation is based on axes of genetic differentiation within populations (see Materials and Methods and (38) for further details). The blue line represents the observed correlation between phenotype and axis of genetic differentiation.

tion for cold resistance alone. What these factors are, we can only speculate about. Phenotypes are shaped by a mixture of neutral and adaptive processes, with a plethora of trade-offs between traits. Investigating phenotypes at different organismal scales in specific and realistic environments will further elucidate how phenotypes and, ultimately, life-history strategies are shaped.

We speculate that the reduced growth plasticity observed for accessions from colder climates is due to the stronger growth reduction at 16ºC in these accessions compared to accessions from warmer climates. They may well be anticipating winter, whereas accessions from warmer climates do not and hence show a stronger difference between 16ºC and 6ºC.

There is strong evidence from QTL mapping that genetic variation in the CBF2 gene is one of the drivers for adaptation to freezing stress (24, 56). Here we looked at growth phenotypes and did not detect associations with the CBF loci. In the transcriptome analysis we did pick-up a role for CBF and other known cold-acclimation genes. The most significant locus detected in our GWAS analysis (for growth rate in 16ºC) lies in the vicinity of *COL5*, a gene that is part of a leaf growth regulatory network (34) and whose expression is induced by both cold treatment and *CBF1*, *CBF2* and *CBF3* overexpression (30). In our transcriptome data, the *COL5* gene was found in cluster D, showing higher expression in accessions coming from warmer regions. It is however unclear what its exact regulatory role in growth in cold conditions might be. In summary, we detected adaptive differentiation for growth between accessions from warm and cold climates. Our transcriptome data and previous metabolome data suggest that resources are relocated from growth to cold acclimation in accessions from colder regions. This allows these accessions to be fully prepared for the coming of winter.

Materials and Methods

Plant growth and phenotyping.

Seeds of 249 natural accessions (Supplementary Dataset 1) of *Arabidopsis thaliana* described in the 1001 genomes project (27) were sown on sieved (6 mm) substrate (Einheitserde ED63). Pots were filled with 71.5 g ±1.5 g of soil to assure homogenous packing. The prepared pots were all covered with blue mats (57) to enable a robust performance of the high-throughput image analysis algorithm. Seeds were stratified (4 days at 4ºC in darkness) after which they germinated and left to grow for 2 weeks at 21ºC (relative humidity: 55%; light intensity: 160µ$molm^{-2}s^{-1}$; 14 h light). The temperature treatments were started by transferring the seedlings to either 6 °C or 16 °C. To simulate natural conditions temperatures fluctuated diurnally between 16-21°C, 0.5-6°C and 8-16°C for the 21°C initial growth conditions and the 6°C and 16°C treatments, respectively (Figure S1). Light intensity was kept constant at 160µ$molm^{-2}s^{-1}$ throughout the experiment. Relative humidity was set at 55% but in colder temperatures it rose uncontrollably to maximum 95%. Daylength was 9h during the 16°C and 6°C treatments. Each temperature treatment was repeated in three independent experiments. Five replicate plants were grown for every genotype per experiment. Plants were randomly distributed across the growth chamber with an independent randomisation pattern for each experiment. During the temperature treatments (14 – 35 days after stratification), plants were photographed twice a day (1 hour. after/before lights switched on/off), using an RGB camera (IDS uEye UI-548xRE-C; 5MP) mounted to a robotic arm. At 35 days after stratification, whole rosettes were harvested, immediately frozen in liquid nitrogen and stored at -80°C until further analysis. Rosette areas were extracted from the plant images using Lemnatec OS (LemnaTec GmbH, Aachen, Germany) software.

Non-linear modeling.

Non-linear modeling was used to describe plant growth in a minimum number of parameters. In a first step we constructed a simple non-linear model with plant size being explained by either the exponential (equation 1) or the power-law function (equation 2), with individual plant as a random effect for each of the model parameters; M_0, r and β. With β being only present in the power-law model. Models were constructed using the *nlsList* and *nlme* functions from the *nlme* package (3.1.152; (58) for R (4.0.3; (59)). Exponential and power-law *SelfStart* functions were used from (28). Based on Akaike Information Criterion and likelihood ratio test generated by the *anova* function (Table 6), we decided to use the power-law model for further analyses.

	Model	df	AIC	BIC	logLik	Test	L.Ratio	p.value
exponential	1	6	-668551.6	-668488.1	334281.8		-	-
power law	2	10	-870605.0	-870499.1	435312.5	1 vs 2	202061	<0.001

Fig. 6. Anova table for the comparison between the exponential and power-law model with degrees of freedom(df), Akaike Information Criterion (AIC), Bayesian Information Criterion (BIC), log-likelihood (logLik) for each model. The likelihood ratio statistic (L.ratio) and p-value are given for the likelihood ratio test that was used to compare these models.

$$\frac{dM}{dt} = rM \tag{1a}$$

$$M_t = M_0 e^{rt} \tag{1b}$$

$$\frac{dM}{dt} = rM^{\beta} \tag{2a}$$

$$M_t = (M_0^{1-\beta} + rt(1-\beta))^{1/(1-\beta)} \tag{2b}$$

In a second step, we constructed a model with fixed effects for the different power-law parameters. For initial size (M_0) we added accession as fixed effect. Temperature treatment only started from the initial time point onwards, and thus could not have an effect on the initial plant size. The growth rate, on the other hand, should be affected by temperature, therefore we included accession, temperature and their interaction as fixed effects for growth rate (r). No fixed effects were added for β. The idea here is that is an adjustment factor for decreasing growth rates (when $\beta < 1$) with increasing plant sizes, which is general for plant growth, or at least for our data in this case. Individuals nested within experiment were added as random effects for each of the model parameters. The correlation structure intrinsic to measuring the same individuals over time was accounted for by adding the first order continuous autoregressive correlation structure (corCAR1). The estimated fixed effects of this model were then used to obtain initial size estimates for each accession and growth rate estimates for each accession in both temperatures. These estimates were used for all further analyses apart from broad-sense heritability calculations (see below).

Climate correlations.

The different phenotypes were correlated with each of the different (bio)climate variables downloaded from www.worldclim.org (60). Correlations were calculated as Pearson's correlations using the *cor* function in R (4.0.3; (59)). Population structure may confound the correlation between phenotype and climate. Therefore we included additional phenotype-climate correlations with correction for population structure (Figure S4). For the population-structure corrected correlations we used a mixed-effects model as implemented in the *lmekin* function from the *coxme* (2.2.16; (61)) package with phenotype as dependent variable, climate variable as fixed effects and the kinship matrix as random effect. The kinship matrix was based on the SNPs from the 1001 genomes consortium (27), the kinship matrix was calculated using 'mixmogam' (https://github.com/bvilhjal/mixmogam) based on (62). In this analysis, phenotype and climate variables were standardized, so that regression coefficients were comparable to correlation coefficients. Even though the strength and significance of the correlations weaken upon population structure correction, the growth parameters still demonstrate the same pattern, being most strongly correlated with winter temperatures.

Seed size correlations.

We used the seeds produced by (63) and limited our measurements to the set of 123 Swedish accessions that overlapped with our growth dataset. After seed stratification for four days at 4ºC in darkness, mother plants were grown for 8 weeks at 4ºC under long-day conditions (16h light; 8h dark) to ensure proper vernalization. Temperature was raised to 21ºC (light) and 16ºC (dark) for flowering and seed ripening. Seeds were kept in darkness at 16ºC and 30% relative humidity, from the harvest until seed size measurements. For each genotype three replicates were pooled and about 200-300 seeds were sprinkled on 12 x 12cm square, transparent Petri dishes. Image acquisition was performed as described in (64) by scanning dishes on a cluster of eight Epson V600 scanners. The resulting 1200 dpi .tiff images were analyzed in the ImageJ software (2.1.0/1.53c). Images were converted to 8-bit binary images and thresholded with the *setAutoThreshold("Defaultdark")* command, and seed area was measured in mm^2 by running the *Analyse Particles* command (inclusion parameters: $size = 0.04 - 0.25$ $circularity = 0.70 - 1.00$). All scripts used for image processing are available at https://github.com/vevel/seed_size. The variance decomposition for initial size into variance explained by winter temperature and seed size was done with a random effect model where initial size was explained by winter temperature and seed size, using the *lmer* and *VarCorr* functions from the *lme4* package (1.1.27.1; (65)) in R (4.0.3; (59)). The seed size corrected correlation between initial size and winter temperature was estimated with the *lme* function from the *nlme* package (3.1.152; (58) in R (4.0.3; (59)), the correction for seed size was done by including seed size as a random effect.

Transcriptome profiling.

35 days after stratification, rosette tissue of all plants were harvested and flash frozen in liquid nitrogen. Random samples from each replicate experiment for both temperatures were taken for 8 accessions to profile the transcriptome with RNA-sequencing. The 8 accessions were selected to represent the climatic variation in the full panel (Figure S8; Supplemental Dataset 1). Total RNA was extracted using the KingFisher Duo Prime System (Thermo Fisher Scientific) together with a high performance RNA bead isolation kit (Molecular Biology Service, VBC Core Facilities, Vienna). To determine the quantity of RNA samples we used Fluorometer Qubit 4 (Invitrogen) and Qubit RNA BR Kit (Invitrogen). For each sample, 1µg of total RNA was treated with the poly(A) RNA Selection Kit (Lexogen) and eluted in 12µl of Nuclease-Free Water. Libraries were prepared according to the manufacturer's protocol in NEBNext Ultra II Directional RNA Library Prep Kit (New England Bi-

oLabs) and individually indexed with NEBNext Multiplex Oligos for Illumina (New England BioLabs). The quantity and quality of each amplified library were analyzed by using Fragment Analyzer (Agilent) and HS NGS Fragment Kit (Agilent). Libraries were sequenced with an Illumina HiSeq2500 in paired-end mode with read-length of 125bp. Sequencing was performed by the Next Generation Sequencing Facility at Vienna BioCenter Core Facilities (VBCF), member of the Vienna BioCenter (VBC), Austria. Samples were distributed over 4 independent libraries. This was due to failed samples that needed replacement. Detailed info on which samples belong to which library is listed in SRA (https://www.ncbi.nlm.nih.gov/sra/PRJNA807069). Gene expression was quantified by using quasi-mapping in salmon (1.2.1; (66). The salmon indices were built separately for each accession, as we incorporated the SNP variation from the (27) into the reference transcriptome. The heatmap was built using *pheatmap* (1.0.12; (67)) in R (4.0.3; (59)). The clustering was done by complete clustering on Euclidean distances, for both rows and columns. The gene clusters were defined by cutting the dendrogram in 7 groups. With a χ^2-test we tested for overrepresentation of a temperature effect on the expression of the 251 selected cold acclimation genes ($df = 1$) compared to the remaining 18784 background genes. We used the *chisq.test* function in R (4.0.3; (59)). Differential expression analysis was conducted with the *DESeq2* package (1.30.0; (68)) in R (4.0.3; (59)). A full model was used, with expression depending on $replicate + accession + temperature + replicate : temperature + accession : temperature$, after which significance of each model coefficient was defined with a negative binomial Wald test. Differential expression for each accession was then extracted by specifying the respective contrasts using the *lfcShrink* function in *DESeq2* with the adaptive shrinkage estimator (69). Genes were considered differentially expressed when the adjusted p-value was lower than 0.05.

Metabolome profiling.

Besides transcriptome profiling of 8 accessions, we also conducted metabolome profiling on all 249 accessions. Samples for metabolome measurements were taken from the same experiments described in this study and, just like the transcriptome samples, were taken at 25 days after stratification. Results and detailed methodology are described in (29).

Broad-sense heritabilities.

Broad-sense heritabilities (H^2) were calculated as the ratio between phenotypic variation explained by genotype (V_g) and the total phenotypic variation (V_p), which is the sum of V_g and phenotypic variation explained by environment (V_e). These variances were obtained from a mixed model by including accession as a random effect (estimate for V_g). Because our accession estimates were corrected for experiment effects, we removed the variance explained by experiment by including experiment as a fixed effect. In order to estimate the variance within each accession (V_e), the dependent variables in this model were the growth parameter estimates for each individual plant, in contrast to the estimates for each accession that were used in all other analyses. These individual plant estimates were obtained from the same model, but took the random effects into account. The variance explained by accession was then taken as an estimate for V_g, the residual variance was taken as V_e. For initial size we calculated heritability over all experiments, growth rate heritabilities were calculated for each temperature independently. The mixed model was constructed with the *lmer* function in the *lme4* package (1.1.27.1; (65)) in R (4.0.3; (59)).

Genome-wide association mapping.

Genome-wide association mapping was done for each of the growth parameters, in both temperatures and also the temperature response for the growth rate. We used a mixed model with phenotype as dependent variable, genotype as fixed effect and genetic relatedness as random factor. Non-imputed SNPs obtained from the (27) were used as genotypes. This model was run in GEMMA (0.98.3; (70), with kinship matrix calculated as the centered relatedness matrix, as implemented in GEMMA.

Testing for adaptive differentiation.

Adaptive differentiation was tested with the method described by (38) and the accompanying quaint package (0.0.0.9; https://github.com/emjosephs/quaint) in R (4.0.3; (59)). The kinship matrix was calculated using the *make_k* function in the quaint package. Genetic principal components were then calculated from the eigen decomposition of the kinship matrix. Adaptive differentiation of each phenotype along the first 10 principal components was tested with the *calcQpc* function in the quaint package. Principal components 11-248 were used to build the expected phenotypic differentiation under neutrality.

ACKNOWLEDGEMENTS

We would like to thank past and current members of the Nordborg group for their help in setting up and harvesting these experiments. Thanks also to Daniele Filiault for her valuable comments on the manuscript.

Supplementary Information

Scripts can be found in https://github.com/picla/growth_16C_6C/. Scripts for seedsize analysis can be found in https://github.com/vevel/seed_size.

Supplemental Dataset 1. List of all 249 accessions with indication of the 8 accessions used for the transcriptome analysis. Supplemental Dataset 2. Cold acclimation genes and their expression cluster membership as shown in Figure 3.

All RNA-sequecing were uploaded to SRA under http://www.ncbi.nlm.nih.gov/bioproject/807069 All generated phenotyping data are filed under 10.5281/zenodo.6076948

Bibliography

1. Russell Lande. A quantitative genetic theory of life history evolution. *Ecology*, 63(3):607–615, June 1982.
2. Stephen C Stearns. *The evolution of life histories.* Oxford University Press, 1992.

3. Aurélien Estarague, François Vasseur, Kevin Sartori, Cristina C Bastias, Denis Cornet, Lauriane Rouan, Gregory Beurier, Moises Exposito-Alonso, Stéphane Herbette, Justine Bresson, Denis Vile, and Cyrille Violle. Into the range: a latitudinal gradient or a center-margins differentiation of ecological strategies in arabidopsis thaliana? *Ann. Bot.*, 129(3):343–356, February 2022.
4. François Vasseur, Kevin Sartori, Etienne Baron, Florian Fort, Elena Kazakou, Jules Segrestin, Eric Garnier, Denis Vile, and Cyrille Violle. Climate as a driver of adaptive variations in ecological strategies in arabidopsis thaliana. *Ann. Bot.*, 122(6):935–945, November 2018.
5. Kevin Sartori, François Vasseur, Cyrille Violle, Etienne Baron, Marianne Gerard, Nick Rowe, Oscar Ayala-Garay, Ananda Christophe, Laura Garcia de Jalón, Diane Masclef, Erwan Harscouet, Maria Del Rey Granado, Agathe Chassagneux, Elena Kazakou, and Denis Vile. Leaf economics and slow-fast adaptation across the geographic range of arabidopsis thaliana. *Sci. Rep.*, 9(1):10758, July 2019.
6. Margarita Takou, Benedict Wieters, Stanislav Kopriva, George Coupland, Anja Linstädter, and Juliette De Meaux. Linking genes with ecological strategies in arabidopsis thaliana. *J. Exp. Bot.*, 70(4):1141–1151, February 2019.
7. Alejandra Martínez-Berdeja, Michelle C Stitzer, Mark A Taylor, Miki Okada, Exequiel Ezcurra, Daniel E Runcie, and Johanna Schmitt. Functional variants of DOG1 control seed chilling responses and variation in seasonal life-history strategies in arabidopsis thaliana. *Proc. Natl. Acad. Sci. U. S. A.*, 117(5):2526–2534, February 2020.
8. Gordon G Simpson and Caroline Dean. Arabidopsis, the rosetta stone of flowering time? *Science*, 296(5566):285–289, April 2002.
9. Jo Hepworth, Rea L Antoniou-Kourounioti, Rebecca H Bloomer, Catja Selga, Kristina Berggren, Deborah Cox, Barley R Collier Harris, Judith A Irwin, Svante Holm, Torbjörn Säll, Martin Howard, and Caroline Dean. Absence of warmth permits epigenetic memory of winter in arabidopsis. *Nat. Commun.*, 9(1):639, February 2018.
10. Johanna A Bac-Molenaar, Dick Vreugdenhil, Christine Granier, and Joost J B Keurentjes. Genome-wide association mapping of growth dynamics detects time-specific and general quantitative trait loci. *J. Exp. Bot.*, 66(18):5567–5580, September 2015.
11. Elodie Marchadier, Mathieu Hanemian, Sébastien Tisné, Liên Bach, Christos Bazakos, Elodie Gilbault, Parham Haddadi, Laetitia Virlouvet, and Olivier Loudet. The complex genetic architecture of shoot growth natural variation in arabidopsis thaliana. *PLoS Genet.*, 15(4):e1007954, April 2019.
12. Benedict Wieters, Kim A Steige, Fei He, Evan M Koch, Sebastián E Ramos-Onsins, Hongya Gu, Ya-Long Guo, Shamil Sunyaev, and Juliette de Meaux. Polygenic adaptation of rosette growth in arabidopsis thaliana. *PLoS Genet.*, 17(1):e1008748, January 2021.
13. A Forsman. Rethinking phenotypic plasticity and its consequences for individuals, populations and species. *Heredity*, 115(4):276–284, October 2015.
14. Mark Van Kleunen and Markus Fischer. Constraints on the evolution of adaptive phenotypic plasticity in plants, 2005.
15. Hannes Claeys and Dirk Inzé. The agony of choice: how plants balance growth and survival under water-limiting conditions. *Plant Physiol.*, 162(4):1768–1779, August 2013.
16. Michael F Thomashow. PLANT COLD ACCLIMATION: Freezing tolerance genes and regulatory mechanisms. *Annu. Rev. Plant Physiol. Plant Mol. Biol.*, 50:571–599, June 1999.
17. Monica A Hughes and M Alison Dunn. The molecular biology of plant acclimation to low temperature. *J. Exp. Bot.*, 47(3):291–305, March 1996.
18. Donna M Bond, Elizabeth S Dennis, and E Jean Finnegan. The low temperature response pathways for cold acclimation and vernalization are independent. *Plant Cell Environ.*, 34(10):1737–1748, October 2011.
19. N N Artus, M Uemura, P L Steponkus, S J Gilmour, C Lin, and M F Thomashow. Constitutive expression of the cold-regulated arabidopsis thaliana COR15a gene affects both chloroplast and protoplast freezing tolerance. *Proc. Natl. Acad. Sci. U. S. A.*, 93(23):13404–13409, November 1996.
20. P L Steponkus, M Uemura, R A Joseph, S J Gilmour, and M F Thomashow. Mode of action of the COR15a gene on the freezing tolerance of arabidopsis thaliana. *Proc. Natl. Acad. Sci. U. S. A.*, 95(24):14570–14575, November 1998.
21. T Nanjo, M Kobayashi, Y Yoshiba, Y Kakubari, K Yamaguchi-Shinozaki, and K Shinozaki. Antisense suppression of proline degradation improves tolerance to freezing and salinity in arabidopsis thaliana. *FEBS Lett.*, 461(3):205–210, November 1999.
22. Sarah J Gilmour, Audrey M Sebolt, Maite P Salazar, John D Everard, and Michael F Thomashow. Overexpression of the arabidopsis CBF3Transcriptional activator mimics multiple biochemical changes associated with cold acclimation. *Plant Physiol.*, 124(4):1854–1865, December 2000.
23. Teruaki Taji, Chieko Ohsumi, Satoshi Iuchi, Motoaki Seki, Mie Kasuga, Masatomo Kobayashi, Kazuko Yamaguchi-Shinozaki, and Kazuo Shinozaki. Important roles of drought- and cold-inducible genes for galactinol synthase in stress tolerance in arabidopsis thaliana. *Plant J.*, 29(4):417–426, February 2002.
24. C G Oakley, J Ågren, R A Atchison, and others. QTL mapping of freezing tolerance: links to fitness and adaptive trade-offs. *Molecular*, 2014.
25. Sunchung Park, Sarah J Gilmour, Rebecca Grumet, and Michael F Thomashow. CBF-dependent and CBF-independent regulatory pathways contribute to the differences in freezing tolerance and cold-regulated gene expression of two arabidopsis ecotypes locally adapted to sites in sweden and italy. *PLoS One*, 13(12):e0207723, December 2018.
26. Carlos Alonso-Blanco, Concepción Gomez-Mena, Francisco Llorente, Maarten Koornneef, Julio Salinas, and José M Martínez-Zapater. Genetic and molecular analyses of natural variation indicate CBF2 as a candidate gene for underlying a freezing tolerance quantitative trait locus in arabidopsis. *Plant Physiol.*, 139(3):1304–1312, November 2005.
27. 1001 Genomes Consortium. 1,135 genomes reveal the global pattern of polymorphism in arabidopsis thaliana. *Cell*, 166(2):481–491, June 2016.
28. C E Timothy Paine, Toby R Marthews, Deborah R Vogt, Drew Purves, Mark Rees, Andy Hector, and Lindsay A Turnbull. How to fit nonlinear plant growth models and calculate growth rates: an update for ecologists. *Methods Ecol. Evol.*, 3(2):245–256, April 2012.
29. Jakob Weiszmann, Pieter Clauw, Joanna Jagoda, Ilka Reichardt-Gomez, Stefanie Koemeda, Jakub Jez, Magnus Nordborg, Dirk Walther, Thomas Nägele, and Wolfram Weckwerth. Plasticity of the primary metabolome in 241 cold grown arabidopsis thaliana accessions and its relation to natural habitat temperature. preprint on BioRxiv, September 2020.
30. Sunchung Park, Chin-Mei Lee, Colleen J Doherty, Sarah J Gilmour, Yongsig Kim, and Michael F Thomashow. Regulation of the arabidopsis CBF regulon by a complex low-temperature regulatory network, 2015.
31. Jonathan T Vogel, Daniel G Zarka, Heather A Van Buskirk, Sarah G Fowler, and Michael F Thomashow. Roles of the CBF2 and ZAT12 transcription factors in configuring the low temperature transcriptome of arabidopsis. *Plant J.*, 41(2):195–211, January 2005.
32. Girdhar K Pandey, Poonam Kanwar, Amarjeet Singh, Leonie Steinhorst, Amita Pandey, Akhlilesh K Yadav, Indu Tokas, Sibaji K Sanyal, Beom-Gi Kim, Sung-Chul Lee, Yong-Hwa Cheong, Jörg Kudla, and Sheng Luan. Calcineurin B-Like Protein-Interacting protein kinase CIPK21 regulates osmotic and salt stress responses in arabidopsis. *Plant Physiol.*, 169(1):780–792, September 2015.
33. Louisa M Liberman, Erin E Sparks, Miguel A Moreno-Risueno, Jalean J Petricka, and Philip N Benfey. MYB36 regulates the transition from proliferation to differentiation in the arabidopsis root. *Proc. Natl. Acad. Sci. U. S. A.*, 112(39):12099–12104, September 2015.
34. Liesbeth Vercruyssen, Aurine Verkest, Nathalie Gonzalez, Ken S Heyndrickx, Dominique Eeckhout, Soon-Ki Han, Teddy Jégu, Rafal Archacki, Jelle Van Leene, Megan Andriankaja, Stefanie De Bodt, Thomas Abeel, Frederik Coppens, Stijn Dhondt, Liesbeth De Milde, Mattias Vermeersch, Katrien Maleux, Kris Gevaert, Andrzej Jerzmanowski, Moussa Benhamed, Doris Wagner, Klaas Vandepoele, Geert De Jaeger, and Dirk Inzé. ANGUSTIFOLIA3 binds to SWI/SNF chromatin remodeling complexes to regulate transcription during arabidopsis leaf development. *Plant Cell*, 26(1):210–229, January 2014.
35. T Prout and J S Barker. F statistics in drosophila buzzatii: selection, population size and inbreeding. *Genetics*, 134(1):369–375, May 1993.
36. Michael C Whitlock. Evolutionary inference from QST. *Mol. Ecol.*, 17(8):1885–1896, April 2008.
37. K Spitze. Population structure in daphnia obtusa: quantitative genetic and allozymic variation. *Genetics*, 135(2):367–374, October 1993.
38. Emily B Josephs, Jeremy J Berg, Jeffrey Ross-Ibarra, and Graham Coop. Detecting adaptive differentiation in structured populations with genomic data and common gardens. *Genetics*, 211(3):989–1004, March 2019.
39. J P Grime. Primary strategies in plants. *Transactions of the Botanical Society of Edinburgh*, 43(2):151–160, November 1979.
40. Mark Westoby. A leaf-height-seed (LHS) plant ecology strategy scheme. *Plant Soil*, 199(2):213–227, February 1998.
41. H K Hayes and O S Aamodt. Inheritance of winter hardiness and growth habit in crosses of marquis with minhardi and minturki wheats. *J. Agric. Res.*, 35(223):236, 1927.
42. Karl S Quisenberry. *Inheritance of Winter Hardiness, Growth Habit, and Stem-rust Reaction in Crosses Between Minhardi Winter and H-44 Spring Wheats*. U.S. Department of Agriculture, 1931.
43. Yves Castonguay, Serge Laberge, E Charles Brummer, and Jeffrey J Volenec. Alfalfa winter hardiness: A research retrospective and integrated perspective*. In *Advances in Agronomy*, volume 90, pages 203–265. Academic Press, January 2006.
44. Pauline Bristiel, Lauren Gillespie, Liv Østrem, Jennifer Balachowski, Cyrille Violle, and Florence Volaire. Experimental evaluation of the robustness of the growth–stress tolerance trade-off within the perennial grass dactylis glomerata. *Funct. Ecol.*, 32(8):1944–1958, August 2018.
45. Kari Koehler, Alyson Center, and Jeannine Cavender-Bares. Evidence for a freezing tolerance-growth rate trade-off in the live oaks (quercus series virentes) across the tropical-temperate divide. *New Phytol.*, 193(3):730–744, February 2012.
46. Craig Loehle. Height growth rate tradeoffs determine northern and southern range limits for trees. *J. Biogeogr.*, 25(4):735–742, July 1998.
47. Marco A Molina-Montenegro, Jorge Gallardo-Cerda, T S M Flores, and Cristian Atala. The trade-off between cold resistance and growth determines the nothofagus pumilio treeline. *Plant Ecol.*, 213(1):133–142, January 2012.
48. Jessica A Savage and Jeannine Cavender-Bares. Phenological cues drive an apparent trade-off between freezing tolerance and growth in the family salicaceae. *Ecology*, 94(8):1708–1717, August 2013.
49. Ying Zhen, Preeti Dhakal, and Mark C Ungerer. Fitness benefits and costs of cold acclimation in arabidopsis thaliana. *Am. Nat.*, 178(1):44–52, July 2011.
50. Ellen Zuther, Elisa Schulz, Liam H Childs, and Dirk K Hincha. Clinal variation in the non-acclimated and cold-acclimated freezing tolerance of arabidopsis thaliana accessions. *Plant Cell Environ.*, 35(10):1860–1878, October 2012.
51. Matthew A Hannah, Dana Wiese, Susanne Freund, Oliver Fiehn, Arnd G Heyer, and Dirk K Hincha. Natural genetic variation of freezing tolerance in arabidopsis. *Plant Physiol.*, 142(1):98–112, September 2006.
52. Matthew W Horton, Glenda Willems, Eriko Sasaki, Maarten Koornneef, and Magnus Nordborg. The genetic architecture of freezing tolerance varies across the range of arabidopsis thaliana. *Plant Cell Environ.*, 39(11):2570–2579, 2016.
53. Matthias H Hoffmann. Biogeography of arabidopsis thaliana (l.) heynh. (brassicaceae). *J. Biogeogr.*, 29(1):125–134, January 2002.
54. Christina Yim, Emily S Bellis, Victoria L DeLeo, Diana Gamba, Robert Muscarella, and Jesse R Lasky. Climate biogeography of arabidopsis thaliana: linking distribution models, individual performance, and life history. preprint on BioRxiv, March 2022.
55. Jon Agren and Douglas W Schemske. Reciprocal transplants demonstrate strong adaptive differentiation of the model organism arabidopsis thaliana in its native range. *New Phytol.*, 194(4):1112–1122, June 2012.
56. Malia A Gehan, Sunchung Park, Sarah J Gilmour, Chuanfu An, Chin-Mei Lee, and Michael F Thomashow. Natural variation in the c-repeat binding factor cold response pathway correlates with local adaptation of arabidopsis ecotypes. *Plant J.*, 84(4):682–693, November 2015.
57. Astrid Junker, Moses M Muraya, Kathleen Weigelt-Fischer, Fernando Arana-Ceballos, Christian Klukas, Albrecht E Melchinger, Rhonda C Meyer, David Riewe, and Thomas Altmann. Optimizing experimental procedures for quantitative evaluation of crop plant performance in high throughput phenotyping systems. *Front. Plant Sci.*, 5:770, 2014.
58. Jose Pinheiro, Douglas Bates, Saikat DebRoy, Deepayan Sarkar, and R Core Team. nlme: Linear and nonlinear mixed effects models, 2021.

59. R Core Team. R: a language and environment for statistical computing, 2017.
60. Stephen E Fick and Robert J Hijmans. WorldClim 2: new 1-km spatial resolution climate surfaces for global land areas. *Int. J. Climatol.*, 37(12):4302–4315, October 2017.
61. Terry M Therneau. coxme: Mixed effects cox models, 2020.
62. Hyun Min Kang, Jae Hoon Sul, Susan K Service, Noah A Zaitlen, Sit-Yee Kong, Nelson B Freimer, Chiara Sabatti, and Eleazar Eskin. Variance component model to account for sample structure in genome-wide association studies. *Nat. Genet.*, 42(4):348–354, April 2010.
63. Envel Kerdaffrec, Danièle L Filiault, Arthur Korte, Eriko Sasaki, Viktoria Nizhynska, Ümit Seren, and Magnus Nordborg. Multiple alleles at a single locus control seed dormancy in swedish arabidopsis. *Elife*, 5, December 2016.
64. Moises Exposito-Alonso, Claude Becker, Verena J Schuenemann, Ella Reiter, Claudia Setzer, Radka Slovak, Benjamin Brachi, Jörg Hagmann, Dominik G Grimm, Jiahui Chen, Wolfgang Busch, Joy Bergelson, Rob W Ness, Johannes Krause, Hernán A Burbano, and Detlef Weigel. The rate and potential relevance of new mutations in a colonizing plant lineage. *PLoS Genet.*, 14(2):e1007155, February 2018.
65. Douglas Bates, Martin Mächler, Ben Bolker, and Steve Walker. Fitting linear Mixed-Effects models using lme4, 2015.
66. Rob Patro, Geet Duggal, Michael I Love, Rafael A Irizarry, and Carl Kingsford. Salmon provides fast and bias-aware quantification of transcript expression. *Nat. Methods*, 14(4): 417–419, April 2017.
67. Raivo Kolde. pheatmap: Pretty heatmaps, 2019.
68. Michael I Love, Wolfgang Huber, and Simon Anders. Moderated estimation of fold change and dispersion for RNA-seq data with DESeq2, 2014.
69. Matthew Stephens. False discovery rates: a new deal. *Biostatistics*, 18(2):275–294, April 2017.
70. Xiang Zhou and Matthew Stephens. Genome-wide efficient mixed-model analysis for association studies. *Nat. Genet.*, 44(7):821–824, June 2012.

Supplemental data

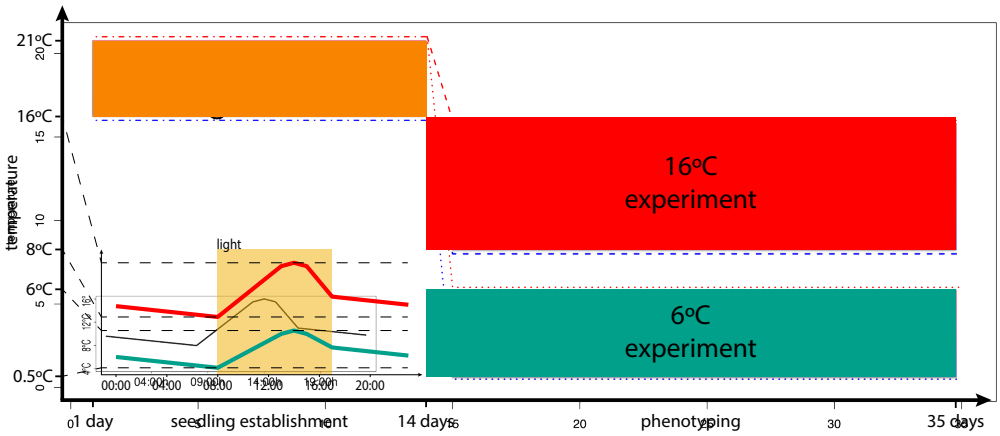

Fig. S1. Timeline of the experiments. Upon stratification, seeds germinated and seedlings established over 14 days. After 14 days plants were exposed to either 16ºC treatment or 6ºC treatment. Insert shows the 24 hour temperature profile for the 16ºC (red) and 6ºC (green) treatments, with light period indicated in yellow.

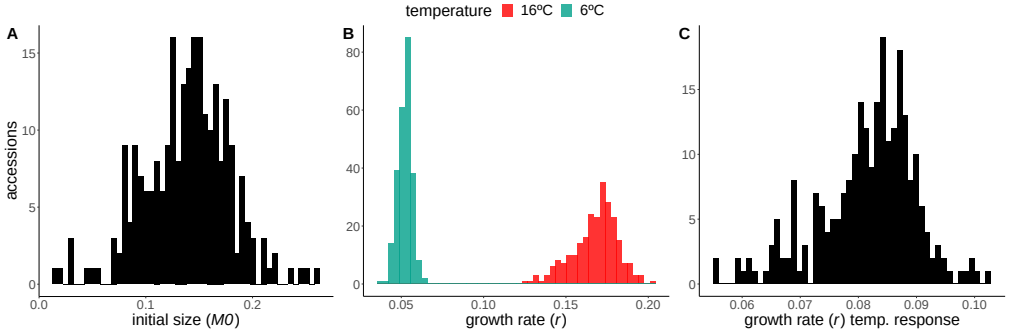

Fig. S2. Variation among accessions of initial size (M_0), growth rate (r) and the temperature response of the growth rate.

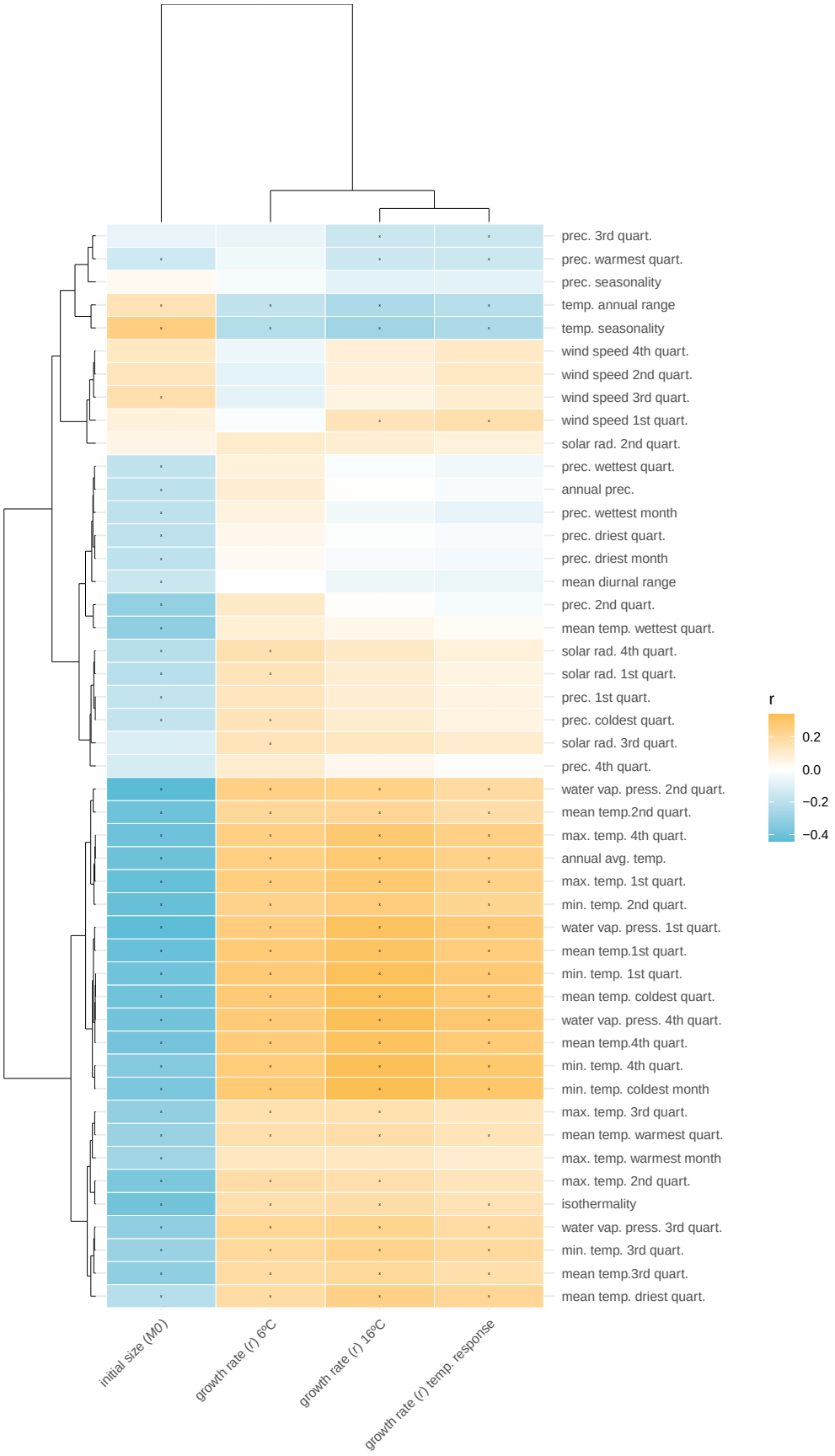

Fig. S3. Correlations between growth parameters and (bio)climate variables. (Bio)climate variables taken from the worldclim database (https://www.worldclim.org). Colors are correlation coefficients, correlations with FDR corrected p-values lower than 0.05 are indicated with a star. The order of the climate variables and phenotypes is based on hierarchical clustering.

Fig. S4. Population structure corrected correlations between growth parameters and (bio)climate variables. (Bio)climate variables taken from the worldclim database (https://www.worldclim.org). Colors are the coefficients for the climate variable in the mixed model with phenotype as dependent variable and population structure as random factor. Phenotypes and climate variables were standardized, making regression coefficients comparable to correlation coefficients. Correlations with FDR corrected p-values lower than 0.05 are indicated with a star. The order of the climate variables and phenotypes is based on hierarchical clustering.

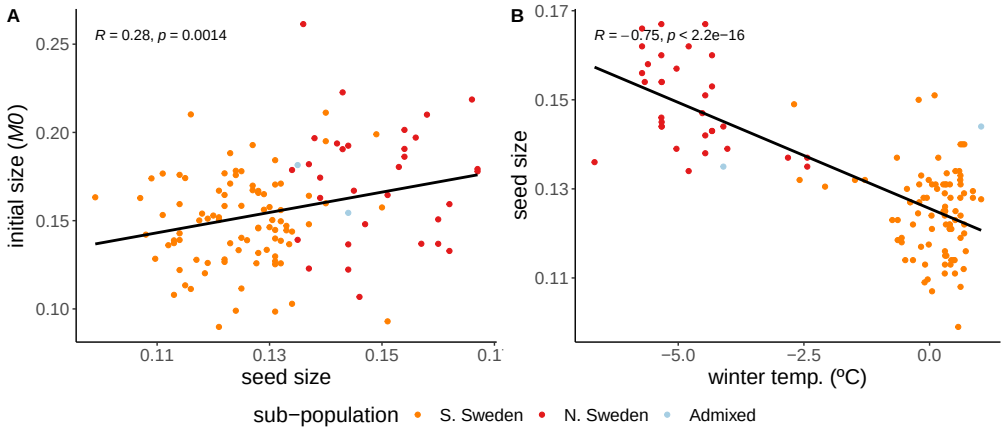

Fig. S5. A: Correlation between initial size and seed size. B: Correlation between seed size and winter temperature. Accessions are a subset of 123 Swedish accessions.

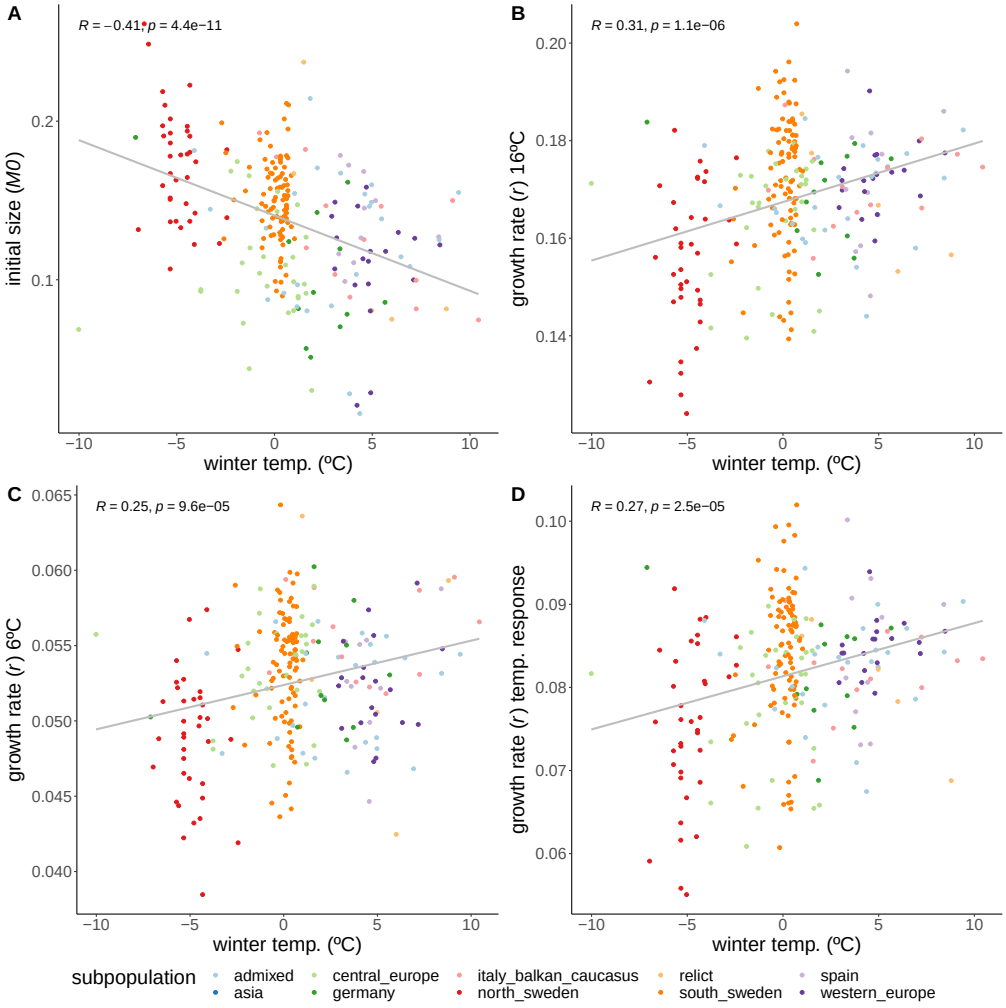

Fig. S6. Correlations of growth parameters with winter temperature, excluding accessions defined as Asian subpopulation. Colors indicate genetically defined subpopulations of the accessions (27).

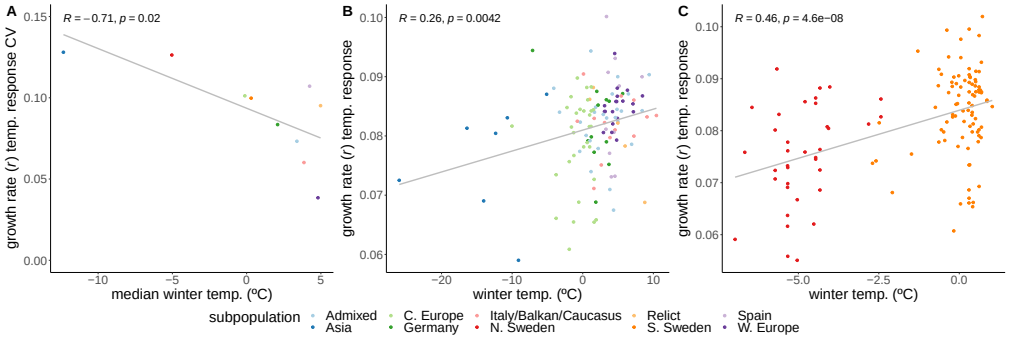

Fig. S7. Growth rate's temperature response variation. A: Coefficient of variance of the growth rate's temperature response, for each subpopulation, correlated with each subpopulation's respective median winter temperature. B: Correlation between growth rate's temperature response and winter temperature, excluding all Swedish accessions. C: Correlation between growth rate's temperature response and winter temperature, exclusively for Swedish accessions.

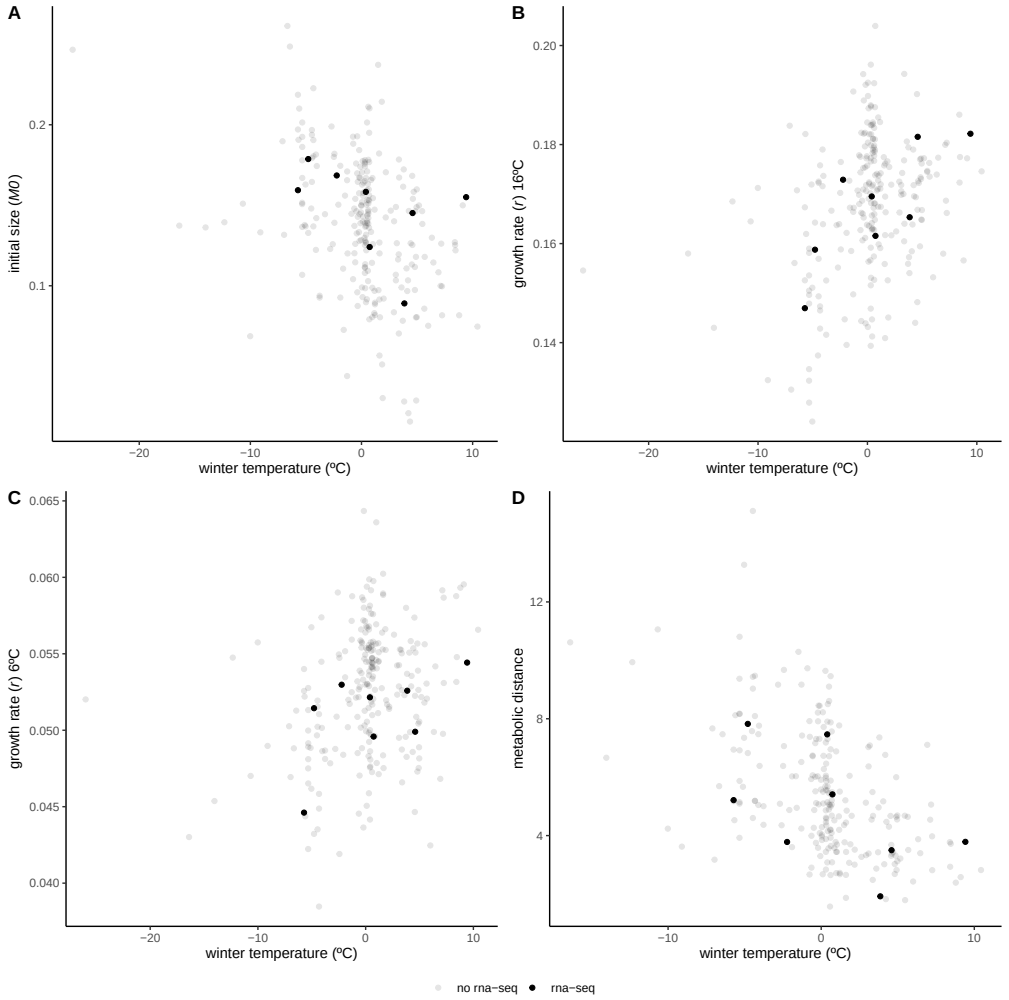

Fig. S8. Growth parameters and metabolic distance of rna-sequenced accessions in relation to local mean temperature of coldest quarter. Initial size (A), growth rate in 16ºC (B) and 6ºC (C), and metabolic distance (D), as a measure of temperature response over all 37 measured primary metabolites (29). Accessions selected for RNA-sequencing are depicted in black, remaining accessions are shown in gray. These 8 accessions were chosen to represent the climatic variation in the full panel.

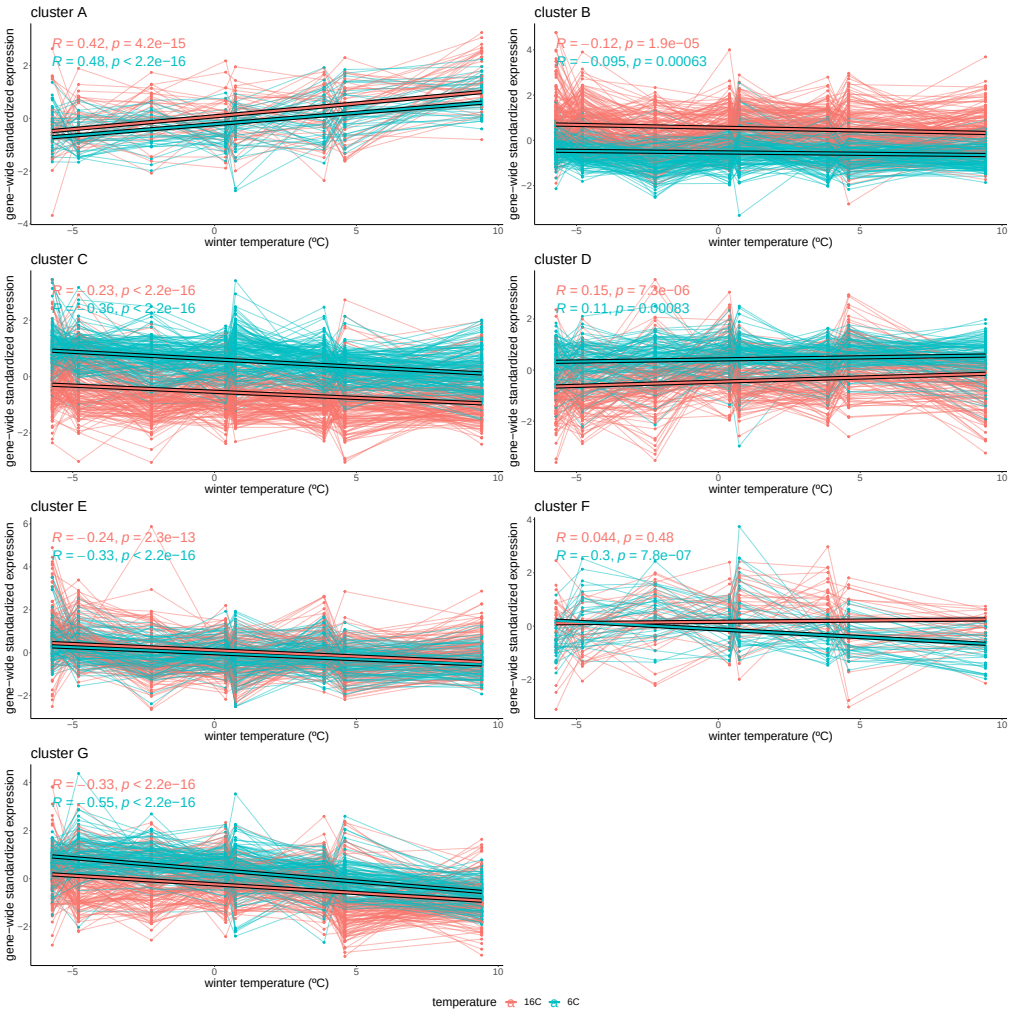

Fig. S9. Cluster-specific expression in relation to winter temperature. Gene-wide standardized expression in 16ºC (red) and 6ºC (blue) values are plotted for each gene in clusters 1-7 (A-G), as defined in Figure 3. Expression values of each gene are connected with thin lines. Thick lines represent the correlation of the cluster's expression with the accession's winter temperature.

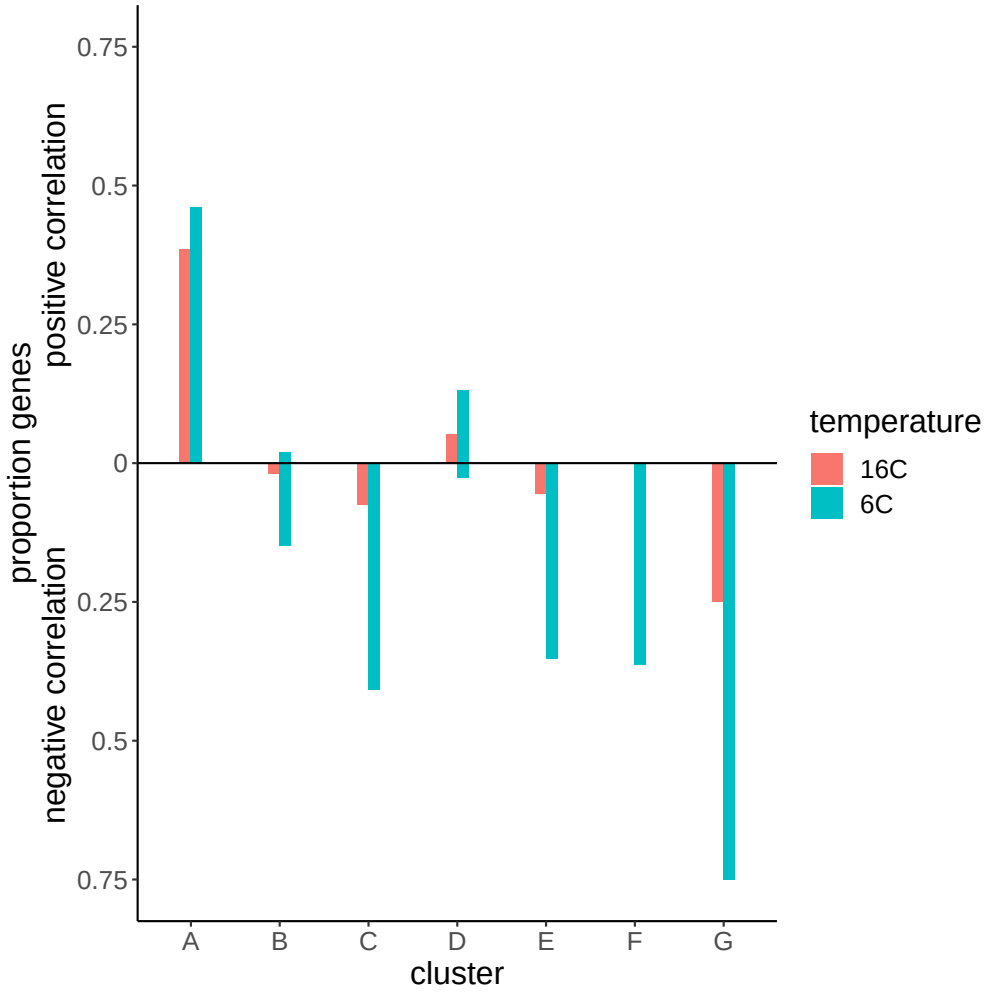

Fig. S10. Proportion of genes in each cluster for which expression significantly correlated with winter temperature ($fdr < 0.05$). Colors indicate the temperature in which expression was measured. Bars above the zero-line are proportions of genes in each cluster that showed a positive correlation with winter temperature. Bars below the zero-line represent proportions of genes that were correlated negatively with winter temperature.

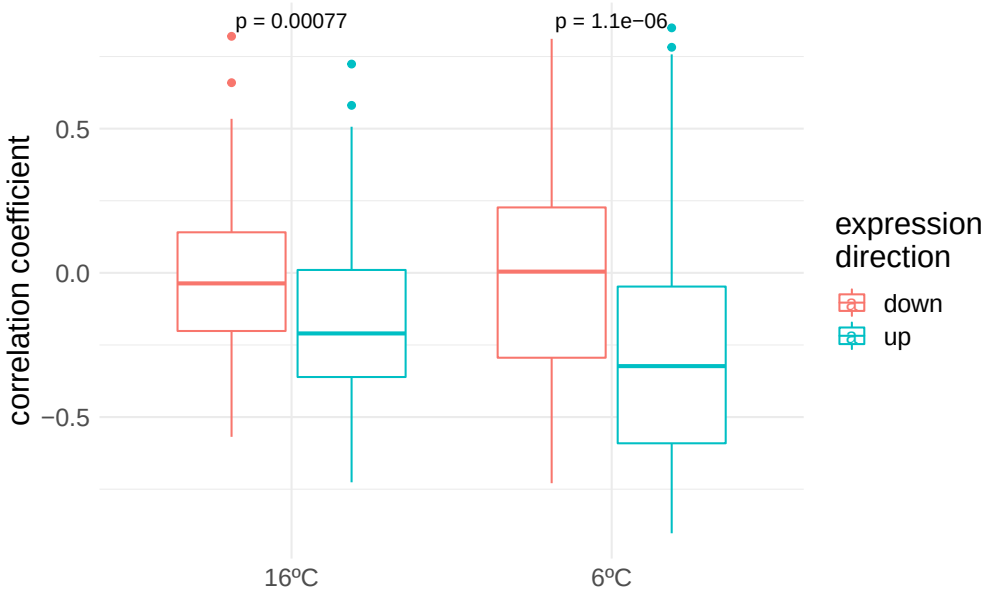

Fig. S11. Gene expression correlations with winter temperature. Correlation coefficients of each gene's correlations with winter temperature are grouped by the experimental temperature (16ºC and 6ºC) and by the expression direction upon cold exposure as measured by (30) (31).

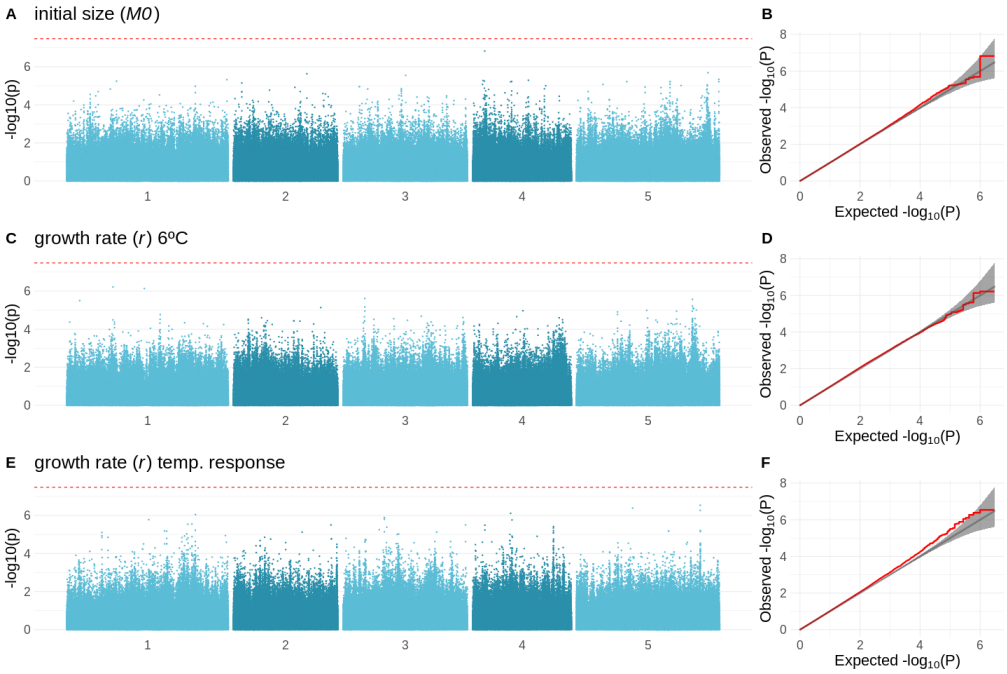

Fig. S12. GWAS results for the initial size, growth rate at 6ºC and the temperature response of the growth rate. Left: Manhattan plots showing the significance of the association between the initial size, growth rate in 6ºC and the growth rate's temperature response, and each of the tested SNPs. The bonferroni-corrected threshold is visualized with the dashed red line. Right: QQ-plots showing the relation between observed and expected $-log10(p-value)$ distributions for each of the respective GWAS. Red line shows the observed relationship. Gray line and band show the expected relationship under the null hypothesis of no differentiation between both distributions.

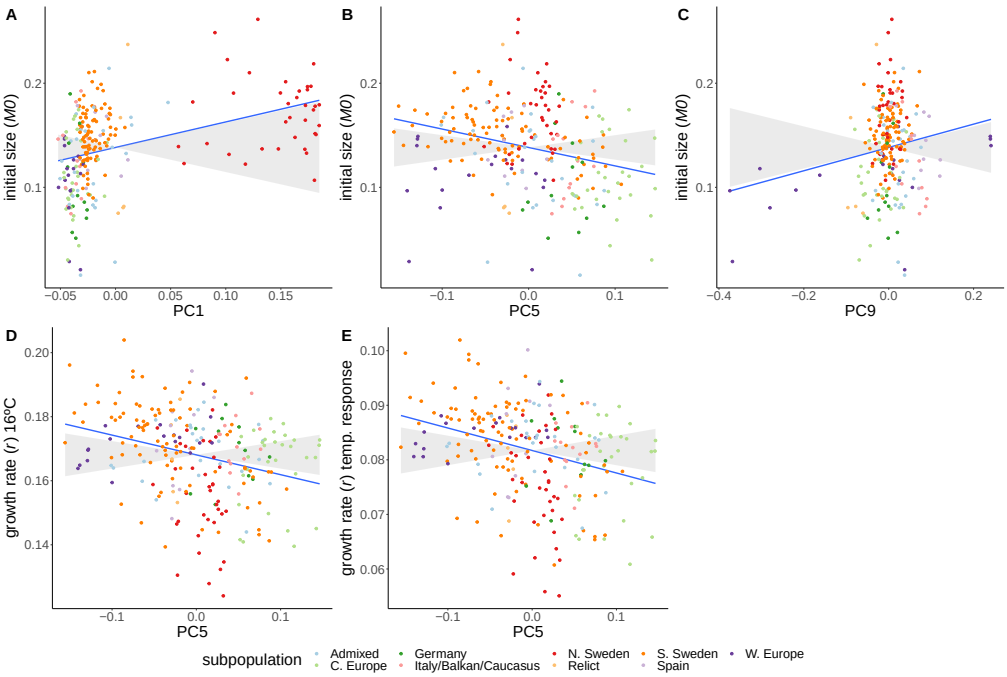

Fig. S13. Adaptive differentiation of initial size, growth rate at 16ºC, and the temperature response of growth rate along different axes of genetic differentiation. Asian accessions were excluded from this analysis to look at their importance to detect adaptive differentiation. Accessions are coloured according to their respective admixture groups, as specified in (27). The gray ribbon represents the expected correlation between phenotype and axis of genetic differentiation under neutrality with a 90% confidence interval. The neutral expectation is based on axes of genetic differentiation within populations (see materials and methods and (38) for further details). The blue line represents the observed correlation between phenotype and axis of genetic differentiation.